

Estimation of Mechanical Properties from Gated SPECT and Cine MRI Data Using a Finite-Element Mechanical Model of the Left Ventricle

Bing Feng, *Student Member, IEEE*, Alexander I. Veress, *Member, IEEE*, Arkadiusz Sitek, *Member, IEEE*, Grant T. Gullberg, *Senior Member, IEEE*, and Dilip Ghosh Roy

Abstract—A significant challenge in diagnosing cardiac disease is determining the viability of myocardial tissue when evaluating the prognosis of vascular bypass surgery. A finite-element mechanical model of the left ventricular myocardium was developed to evaluate mechanical properties of the myocardium, which is an important indicator of viable myocardial tissue and of several aspects of congestive heart failure. The model of the heart muscle mechanics was derived from the passive and active behavior of skeletal muscle, which is considered to be a quasi-incompressible transversely isotropic hyperelastic material of a specified helical fiber structure configuration. Contraction of the myocardium was replicated by simulating active contractions along the helical fibers, then solving (quasi-statically) for the associated boundary valued problem at a sequence of time steps between end-diastole and end-systole of the cardiac cycle. At each time step, the finite-element software package ABAQUS was used to determine the deformation of the left ventricle, which was loaded by intraventricular pressure. An ellipsoidal and a cylindrical model of the left ventricle were developed under both passive loading and active contraction. Parameters that describe the material properties of the myocardium were estimated for the cylindrical model by fitting the radial motion described by the model to gated SPECT and cine MRI data. We found that the estimation was sensitive to the measurement of the motion. Results from the finite-element analysis were compared to those from a purely mathematical description of the cylindrical model.

Index Terms—Cine MRI, finite element, gated cardiac SPECT, left ventricle mechanical model, myocardial mechanical properties.

I. INTRODUCTION

IN THE past few decades, numerous mechanical models of the left ventricle have been developed [1]–[14]. In developing those models, assumptions were usually made about the geometry, fiber orientation, and constitutive equations. Then the boundary valued problem is solved, from which the motion of the left ventricle can be predicted and compared with actual data. Utilizing that data, an evaluation can be made about the accuracy of the original assumptions. The most challenging task is finding the correct constitutive equation for the myocardium.

Mechanical properties of the myocardium are an important indicator of viable myocardial tissue and of congestive heart failure. In particular, knowing the mechanical properties of the myocardial tissue can help in determining viable myocardial tissue when evaluating the prognosis of vascular bypass surgery. Reliable measurements of the mechanical properties of myocardial tissue are difficult to obtain since *ex vivo* uniaxial and biaxial experiments performed on sections of myocardial tissue can give measurements of the mechanical properties that are different from the properties of the intact myocardium. Also, it has been found that measurements taken using different loading protocols generally derive different results [3]. Because of these experimental limitations, various mechanical models of the left ventricle have been developed to investigate the properties of the intact myocardium and fiber orientation [15]–[17]. These mechanical models were used to estimate the mechanical properties of the myocardium utilizing the measured motion of the left ventricle.

Here, a finite-element model of the three-dimensional (3-D) deformation of the left ventricular myocardium is developed and used to simulate the motion of the midventricle during a cardiac cycle. A cylindrical geometry is assumed for the midventricular section of the left ventricle in the finite-element analysis. Though an ellipsoidal model can better predict the correct twisting, a cylindrical model can provide adequate information about the radial motion [17]. Overall, a cylindrical model provides a good approximation of the midventricular section of the left ventricle and gives a good approximation for the radial motion of the midventricular section. We will concentrate on that region in this paper.

The material model of the myocardium is based upon the local mechanical properties of the myocardium and the geometrical configuration of its helical fiber structure. The constitutive equation defining the myocardium is derived from the passive and active behavior of skeletal muscle, which is considered to be a quasi-incompressible transversely isotropic hyperelastic material [18]. The myocardial muscle and skeletal muscle have similar ultrastructures: Each cell consists of sarcomeres, containing interdigitating thick myosin filaments and thin actin filaments. The basic mechanism of contraction is similar in both [19]. However, there are differences. For instance, heart cells act as a whole (all-or-none response), whereas skeletal muscle has a graded contraction of different cells. Another difference is the much larger number of mitochondria and more capillary blood vessels in myocardial muscle, both the direct result of energy

Manuscript received December 8, 2000; revised April 16, 2001. This work was supported in part by the National Institutes of Health under Grant ROI HL39792 and in part by Marconi Medical Systems, Inc.

B. Feng, A. I. Veress, and G. T. Gullberg are with the Medical Imaging Research Laboratory, University of Utah, Salt Lake City, UT 84108-1218 USA.

A. Sitek is with the Lawrence Berkeley National Laboratory, Berkeley, CA 94720 USA.

D. G. Roy is with the U.S. Naval Research Laboratory, Landover, MD 20785 USA.

Publisher Item Identifier S 0018-9499(01)05272-8.

needs that require immediate supply of oxygen and substrate for its metabolic machinery. Mechanically, the most important difference is the resting tension [19]. Overall, a similar mechanical model of a quasi-incompressible transversely isotropic hyperelastic material can be used. However, the differences between cardiac and skeletal muscle must be considered.

The contraction of the myocardium is replicated by simulating active contraction along the helical fibers, then solving (quasi-statically) for the associated boundary value problem at a sequence of time steps between end-diastole and end-systole of the cardiac cycle. At each time step, the finite-element software package ABAQUS¹ is used to determine the deformation of the left ventricle which is loaded by intraventricular pressure.

First, we define the constitutive properties that are assumed in our mechanical model of the myocardium. A mathematical cylindrical model of the midventricular region of the myocardium, based upon the work of Guccione *et al.* [17], is then developed using these constitutive properties. The material constants for the passive myocardium are estimated from MRI data using the mathematical model. The finite-element implementation of the cylindrical model is then presented using the finite-element software package ABAQUS. A parameter that describes the extent of the active contraction is estimated for the contracting left ventricle from both MRI and SPECT data by using ABAQUS

II. CONSTITUTIVE EQUATION

Here, constitutive equations are presented for a mechanical model of the left ventricle of the myocardium. It is shown that the expression for passive loading can be modified to include active contraction.

A. Passive Loading

An important step in defining a mechanical model of a material is the specification of the stress-strain relationship. These relationships are denoted as the constitutive properties of the material. For a hyperelastic material, its mechanical property is uniquely determined by its strain-energy density. From the strain-energy density, the stress-strain relationship can be calculated.

A nearly incompressible version of Humphrey and Yin's model [3] for passive myocardial behavior is proposed. Based on histological observations, they assumed that certain soft tissues consisted of various noninteracting families of densely distributed thin hyperelastic extensible fibers and a homogeneous matrix. The strain-energy density (energy per unit volume) can be described as

$$U = U_I(\bar{I}_1^C) + U_f(\bar{\lambda}_f) + U_J(J) \quad (1)$$

where U is the strain-energy density, which is the sum of

$$U_I = c\{\exp(b(\bar{I}_1^C - 3)) - 1\} \quad (2)$$

$$U_f = A\{\exp(a(\bar{\lambda}_f - 1)^2) - 1\} \quad (3)$$

$$U_J = \frac{1}{D}(J - 1)^2 \quad (4)$$

where

- U_I strain-energy density for the isotropic material matrix;
- U_f strain-energy density for the fiber structures;
- U_J strain-energy density for the related volume change.

The material constants a , b , c , and A depend on the material specimen and the loading protocol. Generally, an increase in b and c increases the stiffness of the isotropic matrix, while an increase in A and a similarly increases the stiffness of the fiber family. The determinant J of the deformation gradient F is equal to one for an incompressible material. (However, in the finite-element implementation, J is not constrained to exactly one, which sometimes is called "nearly incompressible.") $\bar{\lambda}_f$ denotes the fiber stretch ratio and \bar{I}_1^C is the first invariant of the right Cauchy–Green tensor $C = F^T F$. The short bar distinguishes these quantities from their actual values by associating them with the normalized deformation gradient tensor instead of the actual deformation gradient tensor.

The Cauchy stress tensor σ can be calculated from the strain energy as

$$\sigma = \frac{1}{J} \left[U_I' \left(2\bar{B} - \frac{2}{3}\bar{I}_1^C \mathbf{I} \right) + U_f'(\bar{\lambda}_f(n \otimes n)) - \frac{1}{3}\bar{\lambda}_f \mathbf{I} \right] + U_J' \mathbf{I} \quad (5)$$

where \otimes denotes the tensor product. \bar{B} is the normalized left Cauchy–Green tensor, which equals

$$J^{-(2/3)}B = J^{-(2/3)}FF^T \quad (6)$$

with F denoting the deformation gradient tensor. n is the unit vector along the current fiber direction, which can be calculated from the undeformed fiber direction N by

$$n = J^{-(1/3)} \frac{FN}{\bar{\lambda}_f}. \quad (7)$$

I is the second-order unit tensor. The following gives the meaning of the derivatives in (5):

$$U_I' = \frac{\partial U_I}{\partial \bar{I}_1^C} \quad (8)$$

$$U_f' = \frac{\partial U_f}{\partial \bar{\lambda}_f} \quad (9)$$

$$U_J' = \frac{\partial U_J}{\partial J}. \quad (10)$$

B. Active Contraction

The constitutive model developed by Martins *et al.* [4] for active behavior of skeletal muscles is applied. The model extends Humphrey and Yin's model [3] by incorporating Hill's model [20] of active contraction for a one-dimensional segment of muscle fiber in order to derive a three-dimensional model of active contraction for myocardial tissue. Using Hill's model [20], a similar expression to that in (1) for the strain-energy density is derived through the introduction of a nondimensional quantity ξ^{CE} , which is proportional to the strain of the contractile element. This quantity is used as a time-varying input for

¹Hibbit, Karlsson & Sorensen, Inc., Pawtucket, RI.

the model of active contraction. The total strain-energy density per unit volume is given by

$$U = U_I(\bar{I}_1^C) + U_f(\bar{\lambda}_f, \xi^{CE}) + U_J(J) \quad (11)$$

where $U_f(\bar{\lambda}_f, \xi^{CE})$ is the modified strain-energy density for the fiber structures and is defined in [18].

III. MATHEMATICAL CYLINDRICAL MODEL

For a complicated material model with a transmurally varying fiber angle, an analytical solution defining the deformation of the left ventricle is difficult to obtain. Simplifications of the kinematics must be made to reduce the problem to solving a few integral equations. The closest thing to an analytical solution was presented by Guccione *et al.* [17]. They proposed that a cylindrical model be used to represent the midventricular region of the left ventricle. In their model, simplifications of the geometry (a cylinder) and its kinematics were made so that the parameters describing the deformation could be solved numerically.

In their model, a cylindrically symmetric deformation (inflation, stretch, torsion, azimuthal, and axial shear) was then prescribed to simulate the effects of passive loading and active contraction. The strain energy used in their model was quite complicated and difficult to implement into ABAQUS. In our cylindrical model, we utilized the kinematic assumptions from Guccione's model. The cylindrically symmetric deformation of the left ventricle was composed of inflation, stretch, torsion, and azimuthal shear. The current coordinates of the point (r, θ, z) are related to its undeformed coordinates (R, Θ, Z) by the following equations:

$$r = \sqrt{(R^2 - R_1^2)/\lambda + r_1^2} \quad (12)$$

$$\theta = \Theta + \beta Z + \alpha R \quad (13)$$

$$z = \lambda Z. \quad (14)$$

The parameters α, β, λ , and r_1 describe azimuthal shear, torsion, stretch, and deformed inner radius, respectively. They are assumed to be constant and can be calculated by solving the quasi-static equilibrium equation $\nabla \cdot \sigma = 0$. To calculate the Cauchy stress σ , we must know the strain-energy density U and deformation gradient F . The constitutive equations (1) and (5) are used for describing the myocardial behavior for passive loading and for active contraction. From (12)–(14), the deformation gradient tensor is obtained with the following matrix of components in cylindrical coordinates:

$$F = \begin{bmatrix} \frac{\partial r}{\partial R} & \frac{1}{R} \frac{\partial r}{\partial \Theta} & \frac{\partial r}{\partial Z} \\ r \frac{\partial \theta}{\partial R} & \frac{r}{R} \frac{\partial \theta}{\partial \Theta} & r \frac{\partial \theta}{\partial Z} \\ \frac{\partial z}{\partial R} & \frac{1}{R} \frac{\partial z}{\partial \Theta} & \frac{\partial z}{\partial Z} \end{bmatrix} = \begin{bmatrix} \frac{\partial r}{\partial R} & 0 & 0 \\ \alpha r & \frac{r}{R} & \beta r \\ 0 & 0 & \lambda \end{bmatrix}. \quad (15)$$

The normalized left Cauchy–Green tensor is

$$\bar{B} = B = \begin{bmatrix} \left(\frac{\partial r}{\partial R}\right)^2 & \alpha r \left(\frac{\partial r}{\partial R}\right) & 0 \\ \alpha r \left(\frac{\partial r}{\partial R}\right) & (\alpha r)^2 + \left(\frac{r}{R}\right)^2 + (\beta r)^2 & \lambda \beta r \\ 0 & \lambda \beta r & \lambda^2 \end{bmatrix}. \quad (16)$$

Neglecting external body forces and inertial effects, the quasi-static equilibrium equation is $\nabla \cdot \sigma = 0$. Note that the components of the Cauchy stress tensor in these cylindrical coordinates for this axisymmetric deformation are functions of r alone. The equilibrium equation can be expressed by the following system of differential equations in terms of the components of the stress tensor:

$$\frac{d\sigma_{rr}}{dr} + \frac{\sigma_{rr} - \sigma_{\theta\theta}}{r} = 0 \quad (17a)$$

$$\frac{d\sigma_{r\theta}}{dr} + \frac{2\sigma_{r\theta}}{r} = 0 \quad (17b)$$

$$\frac{d\sigma_{rz}}{dr} + \frac{\sigma_{rz}}{r} = 0. \quad (17c)$$

Integrating (17b) and (17c) gives

$$r^2 \sigma_{r\theta} = r_1^2 \sigma_{r\theta}|_{r=r_1} \quad (18)$$

$$r \sigma_{rz} = r_1 \sigma_{rz}|_{r=r_1}. \quad (19)$$

Since there are no shear forces acting upon the inner and outer surfaces of the cylinder, (18) and (19) will be satisfied automatically on these surfaces. Integrating (17a) gives

$$\sigma_{rr} = \int_{r_2}^r \frac{\sigma_{\theta\theta} - \sigma_{rr}}{r} dr + \sigma_{rr}|_{r=r_2}. \quad (20)$$

Since we treat the cylinder as having closed ends, the net axial force is

$$N_z = 2\pi \int_{r_1}^{r_2} r \sigma_{zz} dr - P\pi r_1^2 = 0. \quad (21)$$

Here P is the intraventricular pressure.

Similarly, the resulting torsional moment around the z -axis of the shear forces on the ending planes is

$$M_z = 2\pi \int_{r_1}^{r_2} r^2 \sigma_{\theta z} dr = 0. \quad (22)$$

To solve (20)–(22) simultaneously, the following sum of squares is minimized:

$$\begin{aligned} & \left(\sigma_{rr} - \left(\int_{r_2}^r \frac{\sigma_{\theta\theta} - \sigma_{rr}}{r} dr + \sigma_{rr}|_{r=r_2} \right) \right)^2 \\ & + \left(2\pi \int_{r_1}^{r_2} r \sigma_{zz} dr - P\pi r_1^2 \right)^2 \\ & + \left(2\pi \int_{r_1}^{r_2} r^2 \sigma_{\theta z} dr \right)^2. \end{aligned} \quad (23)$$

Here the Simplex method [21] was used to minimize (23). We will use this mathematical cylindrical model to estimate the passive material properties from MRI data in Section VI.

IV. FINITE-ELEMENT CYLINDRICAL MODEL

In the mathematical cylindrical model described above, the calculation of the deformation gradient tensor was performed after simplifications had been made to the kinematics. This reduced the differential equilibrium equation $\nabla \cdot \sigma = 0$ to three integral equations [(20)–(22)]. For a more accurate solution to the equilibrium equation $\nabla \cdot \sigma = 0$, the finite-element method should be used.

In the finite-element method, the material region of the problem is divided into many small elements with node points. In our application, the nodal displacements are the primary variables. For a nonnodal point in an element, its displacement is calculated by interpolating between the nodal displacements of the element. The deformation gradient tensor is calculated numerically for each point as a function of the displacements of the nodal points.

The software package ABAQUS was used for the finite-element implementation of the cylindrical model of the equatorial region of the left ventricle. ABAQUS is a standard finite-element software package that has a user-defined material subroutine that enables users to define their own material models. In the user-defined subroutine, the Cauchy stress tensor σ and the spatial elasticity tensor $D = \partial\sigma/\partial\varepsilon$ (ε is the strain) are calculated for each Gaussian point. Gaussian points subdivide each finite-element into a mesh of points used for numerical calculation. Since the fiber direction changes when the left ventricle deforms, the fiber orientation is also updated at each calculation. In the following section, several examples that were used to test the implementation of passive and active material models are presented.

V. NUMERICAL EXAMPLES

A. Example 1: Humphrey and Yin's Model Applied to a Cube with Passive Loading

To verify the implementation of Humphrey and Yin's constitutive model in ABAQUS, we used a unit length cube (Fig. 1) consisting of eight nodes. The cube is stretched along the fiber direction parallel to the 1-axis and a rigid body rotation is performed simultaneously around one edge. Since the displacement of each node is prescribed, the deformation gradient tensor is known and can be used to calculate the theoretical value of the stress along the fiber direction. This theoretical value is compared with the ABAQUS results (Fig. 2).

B. Example 2: Humphrey and Yin's Model Applied to a Cylindrical Model of the Heart with Passive Loading

After being validated with the cube, the constitutive model was applied to the cylindrical model of the heart's equatorial region. The mesh used for the cylindrical model is shown in Fig. 3. Helical fiber angles were assumed to vary linearly from 60° at the endocardium to -60° at the epicardium [4], [22]. It is assumed that the cylinder is fixed at one end so that effective stretching pressure will be applied to the opposite end of the cylinder when the pressure load is applied inside the cavity. The following three studies were performed using the cylindrical model.

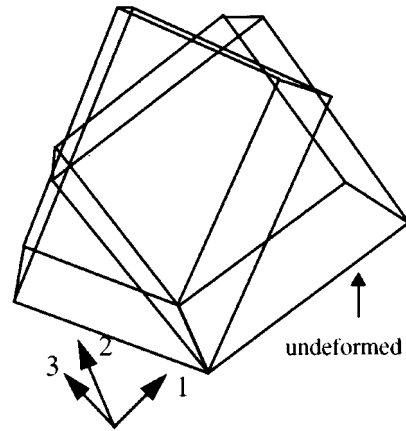


Fig. 1. Mesh used to test the implementation of Humphrey and Yin's model.

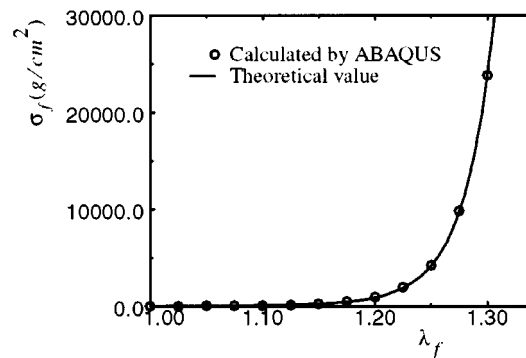


Fig. 2. Comparison of the stress along the fiber direction calculated by ABAQUS with theoretical values.

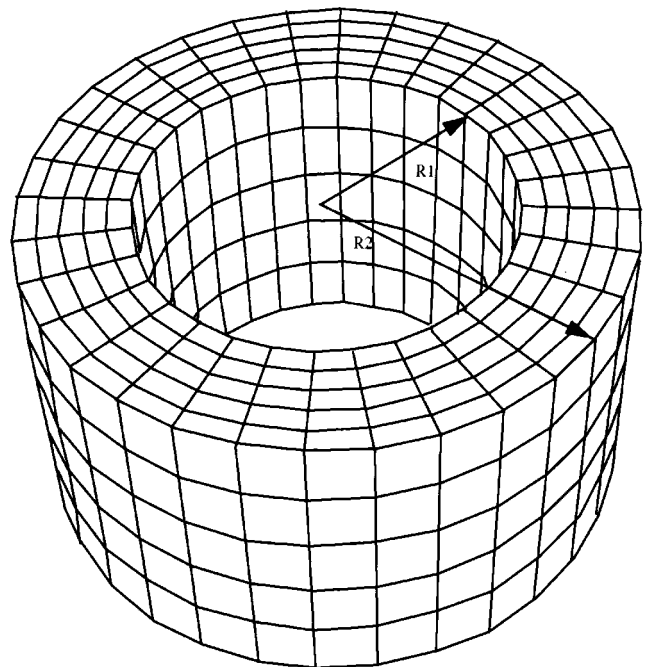


Fig. 3. Mesh used for the cylindrical model of the heart.

1) *Comparison with the Mathematical Cylindrical Model:* Results using ABAQUS were compared to the mathematical cylindrical model proposed by Guccione *et al.*

TABLE I
COMPARISON OF ABAQUS RESULTS WITH CALCULATIONS FROM THE MATHEMATICAL CYLINDRICAL MODEL. (r_1 : INNER RADIUS, β : TWIST, $\varepsilon = \lambda - 1$: ELONGATION OF THE CYLINDER)

P (kPa)	Mathematical			ABAQUS		
	r_1 (cm)	ε	β	r_1 (cm)	ε	β
0	1.720	0	0	1.720	0	0
0.2	1.745	6.4E-4	1.0E-6	1.734	2.3E-4	8.3E-5
0.6	1.796	2.4E-3	2.7E-5	1.761	9.8E-4	2.4E-4
1.2	1.863	5.5E-3	1.4E-4	1.799	2.7E-3	4.3E-4

(see Table I). Both the mathematical model and the finite-element model used the same constitutive properties applied in Humphrey and Yin's model: $a = 12.43$, $b = 23.46$, $A = 5.84$ g/(cm²), and $c = 3.87$ g/(cm²). The results did not compare as well at high pressure (for example, 1.2 kPa) as they did at low pressure. It is hypothesized that the finite-element method provides a better representation of the deformation because more assumptions about the kinematics and boundary conditions are required when specifying the mathematical cylindrical model.

2) *Evaluate the Model Under Different Loading Protocols*: In Humphrey and Yin's paper [3], specimens from different hearts were tested under biaxial loading that used various protocols. The best fit material parameters a , b , A , and c depend on both the specimen and the loading protocol. For example, for specimen #1, the material constants are $a = 234.2$, $b = 19.15$, $A = 0.2536$ g/(cm²), and $c = 5.475$ g/(cm²) under a protocol that keeps the strain ratio between the x and y loading directions during the test at $E_{11}/E_{22} = 1.28$. However, if the loading protocol is changed to $E_{11}/E_{22} = 3.80$, the best fitting parameters are $a = 607.6$, $b = 31.28$, $A = 0.007844$ g/(cm²), and $c = 3.43$ g/(cm²). The two sets of parameters were implemented into the finite-element cylindrical model separately. The results are presented in Table II. It is interesting to note that the loading protocols with different values for E_{11}/E_{22} did not significantly affect the deformation of the heart.

3) *Determining Material Parameters Using MRI Data at End-Diastole*: To match the measurements from a set of MRI data, different specimens from Humphrey and Yin's paper were tested. The results in Table III obtained from specimen #2 in their paper approximately matched cine MRI data at end-diastole. The mechanical properties for this specimen were $a = 382.8$, $b = 11.89$, $A = 0.02649$ g/(cm²), and $c = 0.6151$ g/(cm²).

The MRI data presented in Table III were acquired on a 1.5-T Eclipse MRI scanner² using a sequence that acquired 256×128 images at ten different phases of the cardiac cycle. The sequence parameters were: TE 2.7 ms, bandwidth 31.3 kHz, flip angle 35°, slice thickness 5 mm, and field-of-view 22.5 cm. The sequence acquired two averages of four image phase encodings for each cardiac phase.

²Marconi Medical Systems, Cleveland, OH.

TABLE II
RESULTS FOR SPECIMEN #1 UNDER DIFFERENT LOADING PROTOCOLS ($P = 0.6$ kPa)

E_{11}/E_{22}	r_1 (cm)	ε	β
1.28	1.76	7.6E-4	1.7E-4
3.80	1.76	4.6E-4	1.5E-5

TABLE III
COMPARISON OF ABAQUS RESULTS WITH MRI MEASUREMENTS AT END-DIASTOLE

r_1 (cm)		r_2 (cm)	
Calculated	Measured	Calculated	Measured
1.81	1.91 ± 0.10	2.81	2.84 ± 0.10

The endocardial and epicardial radii were measured from the MRI data at isovolumetric relaxation after end-systole. Regions of interest (ROIs) enclosing the LV cavity and myocardium were then drawn. The software SPECTER³ was used to calculate the enclosed areas, from which the endocardial and epicardial radii were estimated by

$$\text{radius} = \sqrt{\frac{\text{area}}{\pi}}. \quad (24)$$

The process of determining the calculated endocardial (r_1) and epicardial (r_2) radii involved assuming an intraventricular pressure of 0.6 kPa and then changing the material parameters until ABAQUS produced a deformation that gave endocardial and epicardial radii that were close to that of the measured values from the MRI data. Table III gives the best fit for the radii for the material properties given above.

The agreement of the radii values between those calculated by the FE method and the measured values indicates that the assumptions about the material model was reasonable in this case.

C. Example 3: Martin's Model—An Extension of Humphrey and Yin's Model Including Active Contraction

Martin's model of active contraction was tested using a cylindrical bar [Fig. 4(a)] subjected to various activation and inactivation protocols. The material parameters were different than those used in Example 2: $T_0^M = 0.6688$ g/(cm²), $c = 8.21 \times 10^{-4}$ g/(cm²), and $b = 1.79$. In the model for active contraction, the parameters a and A are replaced by the variable T_0^M , which denotes the stiffness of the fiber structure. These values of material constants were applied to an ellipsoidal model of the heart using ABAQUS (Fig. 5). The implementation involved passive loading of 2 kPa followed by an activation of $\xi^{CE} = -5\%$ [Fig. 4(b)]. The heart underwent simultaneous contraction and twisting during the simulation of the cardiac cycle.

VI. EXPERIMENTAL RESULTS—FITTING MRI AND SPECT DATA TO THE MECHANICAL MODEL

Ideally, the image data should provide us with all of the information about the properties of the mechanical model. For ex-

³Copyright 1998 Duke University.

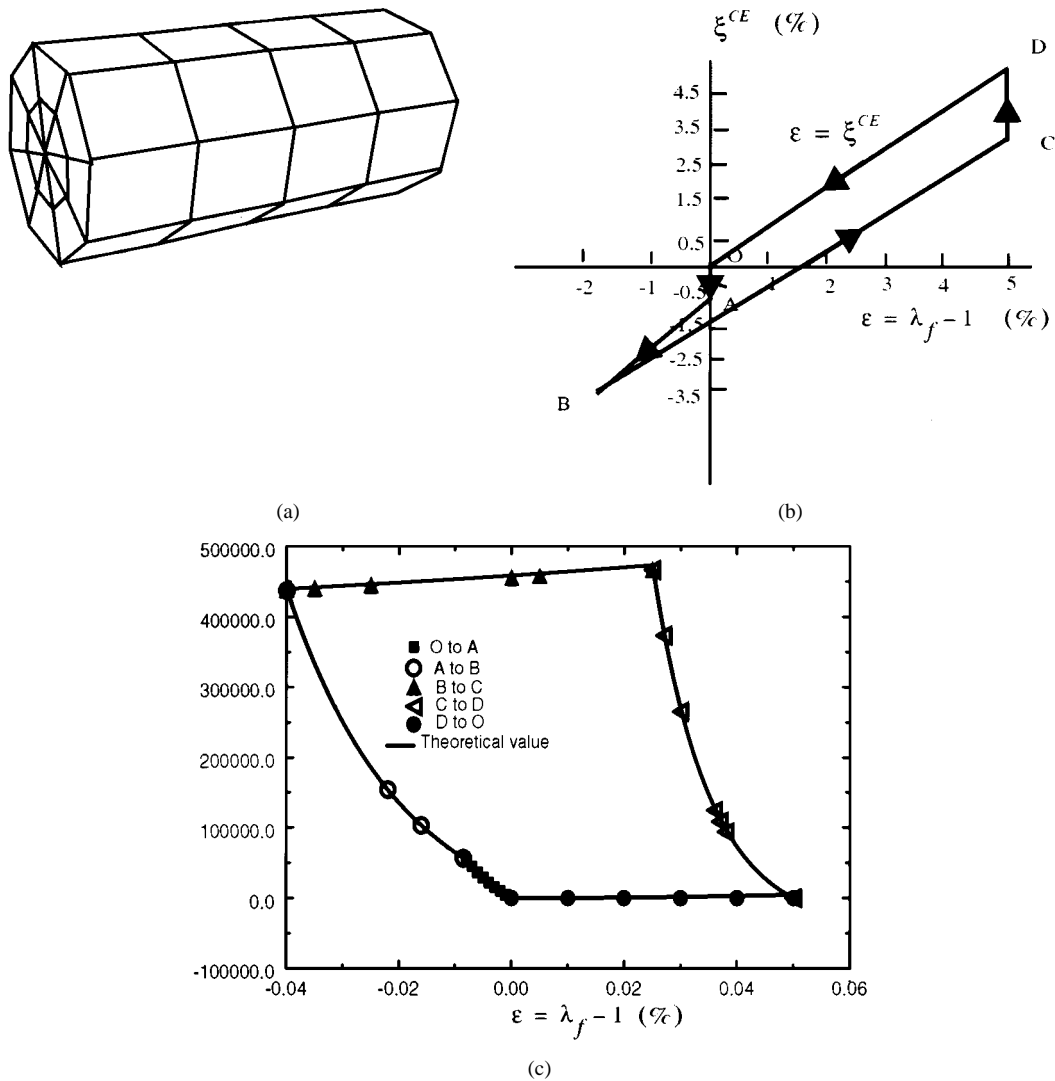


Fig. 4. The (a) geometry, (b) loading protocol, and (c) results validating Martin's model.

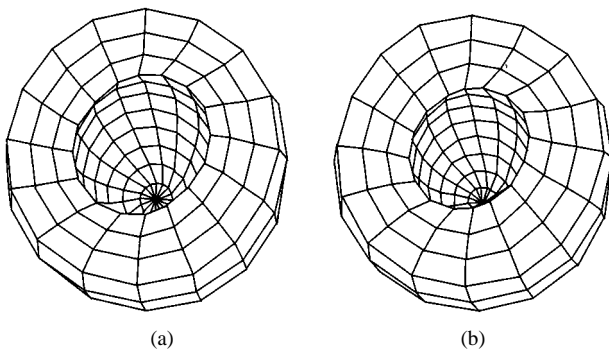


Fig. 5. An ellipsoidal heart model at (a) end-diastole and (b) end-systole.

ample, from 3-D tagged MRI data [23] or from image warping [24], 3-D strain maps can be constructed. Even for SPECT data, it is possible to estimate twisting [25]–[30]. By applying these strain maps to the forward mechanical model, we can fit one or more parameters that describe the fiber structure, material properties, or loading. At present, we do not use fully constructed strain maps. Instead, we fit the radial motion of a midventricular section of the left ventricular wall to a cylindrical mechanical model. From gated SPECT or MRI data (Fig. 6), the inner

and outer radius can be measured during every time frame. Assuming that the material properties, fiber structure, and loading pressure inside the left ventricle are known, we can optimize in a least squares sense the extent of active contraction. This is done by fitting the measured motion of a midventricular section of the left ventricle to the motion specified by the mechanical model.

A. Methods

1) *Motion Derived from MRI and SPECT Data:* In Fig. 7, the endocardial and epicardial radii of a midventricular section of the left ventricle is measured over the entire cardiac cycle. For the MRI data, the inner and outer radii in Fig. 7 were calculated as described in Section V-B3. For the SPECT data, we drew ROIs by setting an activity threshold for the myocardium. Both methods were tested using an MCAT phantom, and strong agreement with known simulated values was obtained.

The intermediate frames a and b between the measured frames 1 and 2 are introduced to simulate the isovolumetric contraction state. Frames c, d, and e between measured frames 4 and 5 are introduced to simulate the relaxation process. To make the seven frames of the MRI data and the eight frames

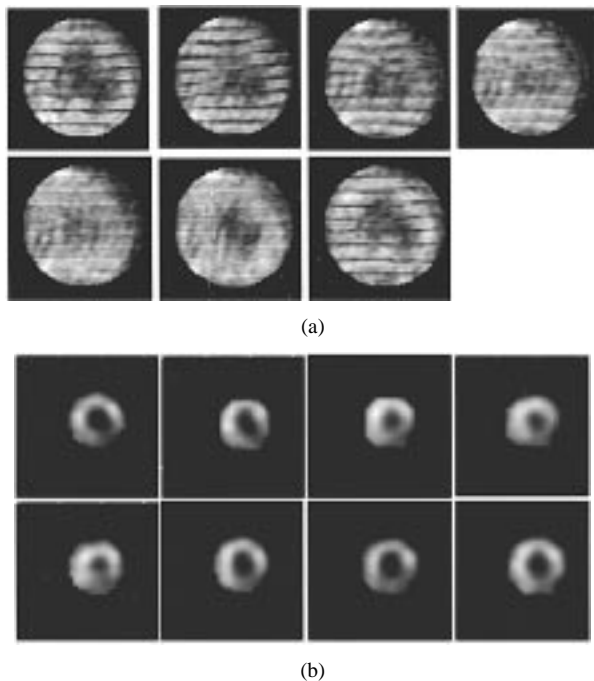


Fig. 6. (a) Seven-frame 1-D tagged MRI data and (b) eight-frame gated SPECT data for the same patient.

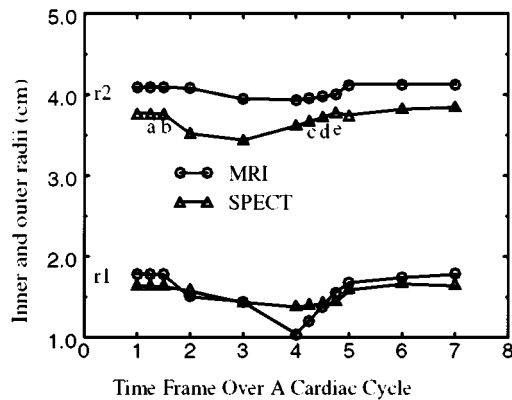


Fig. 7. Fitting the midventricular region of the LV to a cylinder, the inner and outer radii are calculated over a cardiac cycle for both MRI data (circle) and gated SPECT data (triangle).

of the gated SPECT data comparable, it was determined that averaging the fourth and fifth frames of the gated SPECT data into one frame gave frames at comparable time points for seven frames over the cardiac cycle.

2) *Pressure–Time Curve Used in the Analysis:* Since the intraventricular pressure was not measured over a cardiac cycle, a standard pressure–time curve (Fig. 8) is used in all analyses [31].

3) *Material Model:* The mechanical model developed by Martins *et al.* [18] is assumed to represent the left ventricle. This model defines a transversely isotropic, nearly incompressible, hyperelastic material with an adjustable parameter ξ^{CE} that determines the extent of the active contraction. The energy-strain density function is given in (11).

In addition to ξ^{CE} and the local fiber angle, three parameters b , c , and T_0^M describe the material property. Parameters b and c describe the stiffness of the material matrix, while T_0^M describes

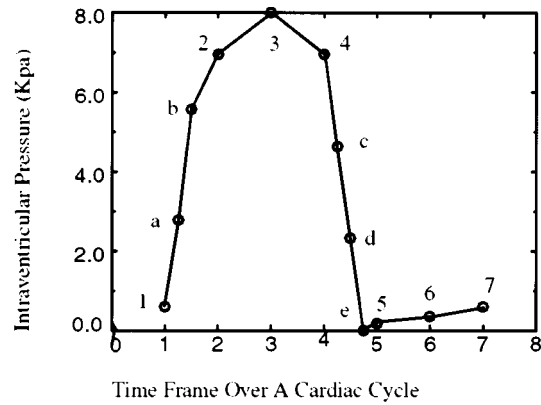


Fig. 8. The assumed intraventricular pressure-time curve over a cardiac cycle. a–e are intermediate frames.

the stiffness of the fiber structure. The fiber angle is assumed to vary linearly along the radial direction across a short slice of the left ventricle wall from 60° at the endocardium to -60° at the epicardium [4], [22].

The values of b , c , and T_0^M were estimated assuming passive behavior of the mechanical model ($\xi^{CE} = 0$). First, Humphrey and Yin’s model [3] was assumed to model the passive behavior of the myocardium. The material properties established in their model were implemented into the mathematical cylindrical model [17]. The best set of material parameters from a table of values in their paper that best predicts the deformation of the LV when compared with the MRI data was then chosen.

In the next step, we used the mathematical cylindrical model to compare Martin’s material model with Humphrey and Yin’s material model. For a range of loading pressures, we calculated the deformations predicted by the mathematical cylindrical model for both materials and tried to estimate the values of b , c , and T_0^M in Martin’s model that minimizes the difference between the total strain energies of the two material models for all loading states. Utilizing this method, we calculated the optimum values of b , c , and T_0^M to be $b = 9.43 \text{ g}/(\text{cm}^2)$, $c = 0.920 \text{ g}/(\text{cm}^2)$, and $T_0^M = 7.09 \times 10^{-2} \text{ g}/(\text{cm}^2)$. These parameters were then used in the material model of (11). The extent of active contraction ξ^{CE} was then estimated from both gated SPECT and cine MRI data by using this material model along with the assumption that the contraction throughout the entire left ventricle wall was uniform.

B. Results

1) *Fitting of MRI and Gated SPECT Data to the Mathematical Cylindrical Model:* Fig. 9 shows estimates of the active contraction parameter ξ^{CE} over the cardiac cycle based upon gated SPECT and cine MRI data. The material deformation described above for the mathematical cylindrical model was assumed. The MRI and SPECT estimates of the extent of active contraction are based on different measurements of the epicardial and endocardial radii throughout the cardiac cycle.

Large differences in the extent of active contraction between the two data sets can be observed at systole in Fig. 9, which is presumably the result of the smaller value of $r1$ at time frame 4 for MRI compared with SPECT in Fig. 7.

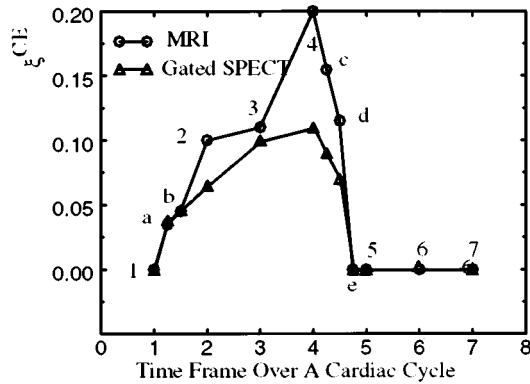


Fig. 9. The absolute value of ξ^{CE} , which describes the extent of the active contraction, is calculated over a cardiac cycle by applying the mathematical cylindrical model to the MRI data (circle) and SPECT data (triangle).

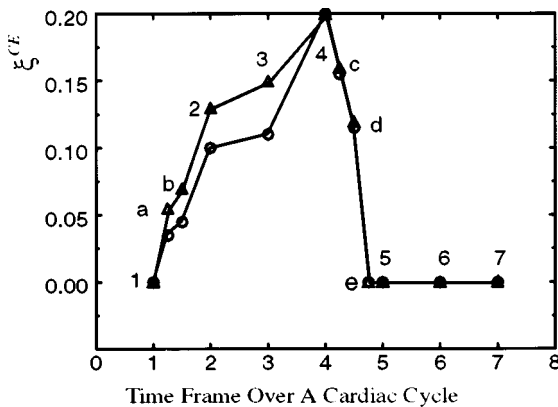


Fig. 10. The extent of active contraction fitted to MRI data. The absolute value of ξ^{CE} , which describes the extent of the active contraction, is calculated over a cardiac cycle by applying the mathematical cylindrical model (circle) and the finite-element model (triangle).

2) *Fitting of MRI Data to the Finite-Element Model:* The same material properties were implemented into a finite-element model by using ABAQUS. To fit the motion of the left ventricle wall derived from MRI data, ξ^{CE} is adjusted at each frame. The results are compared with results obtained using the mathematical cylindrical model shown in Fig. 10.

VII. DISCUSSION

Cylindrical mathematical and finite-element mechanical models of the left ventricle have been presented. Both of these models were fit to gated SPECT and cine MRI data. In fitting the mathematical cylindrical model to image data, passive material properties were obtained. The parameter that describes the extent of the active contraction was determined by fitting the imaging data to a mathematical model and an finite-element model that also included active contraction.

Finite-element analysis is a good tool for modeling the mechanics of the left ventricle. It can manage complex geometries and boundary conditions. Complex material properties can also be implemented into the model. Compared to the mathematical cylindrical model, which requires many assumptions about the kinematics and boundary conditions, the finite-element method provides more accurate results.

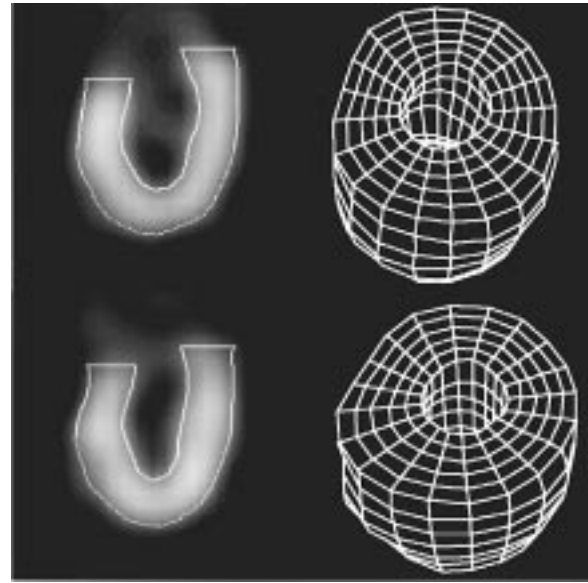


Fig. 11. Finite-element meshes generated from gated SPECT data. (Top) End-diastole and (bottom) end-systole.

The mechanical model is helpful for describing the deformation of the left ventricle. Usually a single imaging modality such as gated SPECT cannot provide information about twist and shear strains. If the material properties and boundary conditions for a mechanical model of the left ventricle are known, then motion can be determined better. In this sense, a mechanical model can provide additional information about the motion of the left ventricle. On the other hand, if the strain map of the left ventricle is available from other sources (such as 3-D tagged MRI imaging, image warping method, etc.), the material properties of the myocardium can also be obtained by fitting the deformation of the left ventricle to the known strain map.

The mathematical cylindrical model was used to estimate the passive material properties of the myocardium from MRI data. The measured values provided by Humphrey [3] were chosen one by one and tested to see which one gave the best fit values. An alternative approach is to perform a least squares fit using the mathematical cylindrical model to estimate the material constants. One problem may be that the results are very sensitive to the input values of the radii at end-diastole. Table II illustrates this sensitivity. Within the measurement accuracy, the motions for two sets of material parameters were nearly the same. This illustrates the sensitivity of the estimation of the activation parameter ξ^{CE} at end-systole (Fig. 9).

In future work, it will be important to develop more realistic geometries of the left ventricle for the mechanical model that is fit to imaging data. Also, in this paper we did not include initial stresses in our model. If a heart is sliced, it will spring open, which is proof of the existence of initial stresses in the undeformed state [17]. For a nonlinear material like the myocardium, lack of knowledge about initial stresses may cause subtle errors in the estimation of its deformation. The correction of the effect of initial stresses may be a difficult problem since it is nonuniform over the left ventricle and may vary significantly from patient to patient.

VIII. FUTURE WORK

Future work will involve using more realistic finite-element meshes derived from the imaging data. We are developing algorithms to automatically generate finite-element meshes from gated SPECT data (see Fig. 11). The use of image-derived meshes should provide both the ability to track the deformation of the left ventricle locally and the ability to fit the motion to the deformation locally. We also propose to fit the motion of the left ventricle to a map of the deformation derived from 3-D tagged MRI data or image warping data to obtain estimates of material properties of the myocardium. We will attempt to include the initial stresses in the model. Finally, we propose to introduce electrical propagation into the finite-element model. In that case, the changing of ξ^{CE} over time and space may be described physiologically, which will lead to a real-time model.

ACKNOWLEDGMENT

The authors would like to thank S. Webb for proofreading the manuscript.

REFERENCES

- [1] T. Arts, R. S. Reneman, and P. C. Veenstra, "A model of the mechanics of the left ventricle," *Ann. Biomed. Eng.*, vol. 7, pp. 299–318, 1979.
- [2] J. M. Huyghe, D. H. van Campen, T. Arts, and R. M. Heethaar, "A two-phase finite element model of the diastolic left ventricle," *J. Biomechs.*, vol. 24, pp. 527–538, 1991.
- [3] J. D. Humphrey and F. C. P. Yin, "On constitutive relations and finite deformations of passive cardiac tissue: I. A pseudostrain-energy function," *ASME J. Biomech. Eng.*, vol. 109, pp. 298–304, 1987.
- [4] P. H. M. Bovendeerd, T. Arts, J. M. Huyghe, D. H. Van Campen, and R. S. Reneman, "Dependence of local left ventricular wall mechanics on myocardial fiber orientation: A model study," *J. Biomechs.*, vol. 25, pp. 1129–1140, 1992.
- [5] T. Arts, W. C. Hunter, A. Douglas, A. M. M. Muijtjens, and R. S. Reneman, "Description of the deformation of the left ventricle by a kinematic model," *J. Biomech.*, vol. 25, pp. 1119–1127, 1992.
- [6] A. McCulloch, J. Guccione, L. Waldman, and J. Rogers, "Large-scale finite element analysis of the beating heart," in *High-Performance Computing in Biomedical Research*, T. C. Pilkington, B. Loftis, J. F. Thompson, S. L. Woo, T. C. Palmer, and T. F. Budinger, Eds. Boca Raton, FL: CRC Press, 1993, pp. 27–49.
- [7] P. J. Hunter, P. M. F. Nielsen, B. H. Smaill, I. J. LeGrice, and I. W. Hunter, "An anatomical heart model with applications to myocardial activation and ventricular mechanics," in *High-Performance Computing in Biomedical Research*, T. C. Pilkington, B. Loftis, J. F. Thompson, S. L. Woo, T. C. Palmer, and T. F. Budinger, Eds. Boca Raton, FL: CRC Press, 1993, pp. 3–26.
- [8] J. M. Guccione and A. D. McCulloch, "Mechanics of active contraction in cardiac muscle: Part I—Constitutive relations for fiber stress that describe deactivation," *Trans. ASME*, vol. 115, pp. 72–81, 1993.
- [9] J. M. Guccione, L. K. Waldman, and A. D. McCulloch, "Mechanics of active contraction in cardiac muscle: Part II—Cylindrical models of the systolic left ventricle," *Trans. ASME*, vol. 115, pp. 82–90, 1993.
- [10] J. M. Guccione, K. D. Costa, and A. D. McCulloch, "Finite element stress analysis of left ventricular mechanics in the beating dog heart," *J. Biomechs.*, vol. 28, pp. 1167–1177, 1995.
- [11] K. D. Costa, P. J. Hunter, J. M. Rogers, J. M. Guccione, L. K. Waldman, and A. D. McCulloch, "A three-dimensional finite element method for large elastic deformations of ventricular myocardium: I—Cylindrical and spherical polar coordinates," *Trans. ASME*, vol. 118, pp. 452–463, 1996.
- [12] ———, "A three-dimensional finite element method for large elastic deformations of ventricular myocardium: II—Prolate spheroidal coordinates," *Trans. ASME*, vol. 118, pp. 464–472, 1996.
- [13] I. J. LeGrice, P. J. Hunter, and B. H. Smaill, "Laminar structure of the heart: A mathematical model," *Amer. J. Physiol.*, vol. 272, pp. H2466–H2476, 1997.
- [14] P. J. Hunter, B. H. Small, P. M. F. Nielsen, and I. J. LeGrice, "A mathematical model of cardiac anatomy," in *Computational Biology of the Heart*, A. V. Panfilov and A. V. Holden, Eds. Chichester, U.K.: Wiley, 1997, pp. 171–215.
- [15] P. J. Hunter, M. P. Nash, and G. B. Sands, "Computational electromechanics of the heart," in *Computational Biology of the Heart*, A. V. Panfilov and A. V. Holden, Eds. Chichester, U.K.: Wiley, 1997, pp. 345–407.
- [16] X. Papademetris, A. J. Sinusas, D. P. Dione, and J. S. Duncan, "Estimation of 3D left ventricular deformation from echocardiography," *Med. Image Anal.*, vol. 5, pp. 17–28, 2001.
- [17] J. M. Guccione, A. D. McCulloch, and L. K. Waldman, "Passive material properties of intact ventricular myocardium determined from a cylindrical model," *ASME J. Biomech. Eng.*, vol. 113, pp. 42–55, 1991.
- [18] J. A. C. Martins, E. B. Pires, R. Salvado, and P. B. Dinis, "A numerical model of passive and active behavior of skeletal muscles," *Comput. Methods Appl. Mech. Eng.*, vol. 151, pp. 419–433, 1998.
- [19] Y. C. Fung, *Mechanical Properties of Living Tissues*, 2nd ed: Biomechanics, p. 427.
- [20] A. V. Hill, "Time heart of shortening and the dynamic constants of muscle," *Proc. Roy. Soc. Biol.*, vol. 126, pp. 136–195, 1938.
- [21] *Numerical Recipe in C*, 2nd ed. New York: Cambridge Univ. Press, ch. 10, pp. 408–412.
- [22] *Handbook of Physiology*, R. M. Berne, Ed., American Physiological Society, Bethesda, MD, 1979, pp. 61–112.
- [23] T. S. Denney, Jr. and E. R. McVeigh, "Model-free reconstruction of three-dimensional myocardial strain from planar tagged MR images," *JMRI*, vol. 7, pp. 799–810, 1997.
- [24] A. Bowden, R. Rabbitt, J. Weiss, and B. Maker, "Use of medical image data to compute strain fields in biological tissue," in *Proc. ASME Bioengineering Conf.*, vol. BED-35, 1997, pp. 191–192.
- [25] K. Nichols, C. D. Cooke, T. L. Faber, E. V. Garcia, M. Kamran, and E. G. DePuey, "Detection of cardiac torque from gated myocardial perfusion tomograms," *J. Nucl. Med.*, vol. 41, p. 45, 2000.
- [26] K. Nichols, M. Kamran, C. D. Cooke, T. L. Faber, E. V. Garcia, and E. G. DePuey, "Correction for torque improves myocardial perfusion quantitation," *JACC*, vol. 37, p. 411A, 2001.
- [27] G. J. Klein, B. W. Reutter, and R. H. Huesman, "Non-rigid summing of gated PET via optical flow," *IEEE Trans. Nucl. Sci.*, vol. 44, pp. 1509–1512, 1997.
- [28] A. Sitek, G. T. Gullberg, D. N. Ghosh Roy, and E. V. R. Di Bella, "Use of imaging data for modeling heart deformation by finite element methods," in *IEEE Nuclear Science Symposium and Medical Imaging Conf. Rec.*, Seattle, WA, Oct. 34–30, 1999, pp. 1566–1568.
- [29] A. Sitek, G. J. Klein, G. T. Gullberg, and R. H. Huesman, "Deformable model of the heart with fiber structure," *IEEE Trans. Nucl. Sci.*, to be published.
- [30] G. J. Klein, "Forward deformation of PET volumes using nonuniform elastic material constraints," in *Information Processing in Medical Imaging, XVth IPMI Int. Conf.*, A. Kuba, M. Samal, and A. Todd-Pokropek, Eds. Visegrad, Hungary, June 28–July 2, 1999, pp. 358–363.
- [31] R. M. Berne and M. N. Levy, *Physiology*. St. Louis, MO: Mosby, 1998, p. 369.